Available online at www.sciencedirect.com
ScienceDirect
Forest Ecology and Management 253 (2007) 220–231
Forest Ecology and Management
www.elsevier.com/locate/foreco

Characterizing spatial–temporal tree mortality patterns associated with a new forest disease

Desheng Liu [a,*], Maggi Kelly [b,c], Peng Gong [c], Qinghua Guo [d]

[a] Department of Geography and Department of Statistics, The Ohio State University, 1036 Derby Hall, 154 North Oval Mall, Columbus, OH 43210-1361, United States
[b] Geospatial Imaging and Informatics Facility, University of California, Berkeley, 111 Mulford Hall, Berkeley, CA 94720-3114, United States
[c] Department of Environmental Science, Management and Policy, University of California, Berkeley, 145 Mulford Hall, Berkeley, CA 94720-3114, United States
[d] School of Engineering, University of California at Merced, P.O. Box 2039, Merced, CA, 95344, United States

Received 1 March 2007; received in revised form 19 July 2007; accepted 19 July 2007

Abstract

A new forest disease called Sudden Oak Death, caused by the pathogen *Phytophthora ramorum*, occurs in coastal hardwood forests in California and Oregon. In this paper, we analyzed the spatial–temporal patterns of overstory oak tree mortality in China Camp State Park, CA over 4 years using the point patterns mapped from high spatial resolution remotely sensed imagery. Both univariate and multivariate spatial point pattern analyses were performed with special considerations paid to the spatial trends illustrated in the mapped point patterns. In univariate spatial point pattern analyses, we investigated inhomogeneous *K*-functions and Neyman–Scott point processes to characterize and model the spatial dependence among dead oak trees in each year. The results showed that the point patterns of dead oak trees are significantly clustered at different scales and spatial extents through time; and that both the extent and the scale of the clustering patterns decrease with time. In multivariate spatial point pattern analyses, we developed two simulation methods to test the spatial–temporal dependence among dead oak trees over time and the spatial dependence between dead oak trees and California bay trees, an important host for the pathogen. The results showed that new dead oak trees tend to be located within up to 300 m of past dead oak trees; and that a strong spatial association between oak tree mortality and California bay trees exists 150 m away.
Published by Elsevier B.V.

Keywords: Sudden Oak Death; Spatial–temporal patterns; Spatial point pattern analysis; Inhomogeneous *K* function; Neyman–Scott point process

1. Introduction

Spatial pattern analysis is a common tool in plant ecology used for detecting spatial patterns of species distribution, understanding interactions between plants and the environment, and inferring important ecological processes or mechanisms of plant population dynamics (Franklin et al., 1985; Welden et al., 1990; Dale, 1999; Goreaud et al., 2002; Arevalo and Fernandez-Palacios, 2003; Schurr et al., 2004). In studying plant disease epidemics, quantifying and understanding the spatial pattern of disease establishment and spread is fundamental to understand disease dynamics because spatial pattern reflects the environmental forces acting on the dispersal and life cycles of a pathogen (Ristaino and Gumpertz, 2000; Suzuki et al., 2003). For this reason, and because plant diseases can operate at large spatial scales, researchers are increasingly using landscape approaches (e.g. remote sensing, spatial statistics) to quantify and model spatial patterns of disease spread in order to understand the basic factors that influence pathogen dispersal and infection processes (Cole and Syms, 1999; Holdenrieder et al., 2004; Wulder et al., 2004).

Many spatial statistical methods have been developed to quantify and model spatial patterns of forest diseases (Reich and Lundquist, 2005). Typically, the locations of unaffected, diseased and dead trees are analyzed for spatial pattern; usually, such populations of trees are represented by various spatial point data derived through field sampling or mapping from remotely sensed imagery. As such, spatial point pattern analysis has been intensively investigated to reveal the scale, extent, and dynamics of mortality patterns and test potential hypotheses related to spatial mechanisms of disease spread. For example, Batista and Maguire (1998) modeled the spatial structure of tree

* Corresponding author. Tel.: +1 614 247 2775; fax: +1 614 292 6213.
E-mail address: liu.738@osu.edu (D. Liu).

0378-1127/$ – see front matter. Published by Elsevier B.V.
doi:10.1016/j.foreco.2007.07.020

mortality as a ''thinning'' process on the existing live trees in tropical stands. Cole and Syms (1999) applied various spatial analysis techniques to differentiate between climate-induced and pathogen-induced mass mortalities of the kelp *Ecklonia radiata* in north-eastern New Zealand. Kelly and Meentemeyer (2002) quantified the scale and extent of spatial clustering of oak mortality in a selected portion of a hardwood forest associated with Sudden Oak Death forest disease using Ripley's *K*-function in California.

Sudden Oak Death (SOD) has been known as a new forest disease in coastal central California and southern Oregon since the middle 1990s. The disease caused by a recently discovered pathogen *Phytophthora ramorum* has been killing hundreds of thousands of tanoak (*Lithocarpus densiflorus*), coast live oak (*Quercus agrifolia*), and black oak (*Quercus kelloggii*) trees (Rizzo et al., 2002; Rizzo and Garbelotto, 2003). The disease has imposed serious impacts on coastal forests in California, and it is necessary to study the disease distribution and spread and provide scientific understanding on the disease dynamics for better disease control and management. Particularly, the spatial behavior of this disease is one of the most important components for us to understand disease dynamics. The trees mentioned above are terminal hosts for the disease, with spread occurring primarily from one or more ''foliar hosts'', such as California bay (*Umbellularia californica*) and Madrone (*Arbutus menziesii*). Recent field studies indicated that these foliar hosts are probably the most durable and persistent source of the pathogen and the pathogen has also been found in rainwater, soil, litter, and streamwater (Davidson et al., 2002, 2005). Short distance pathogen movement is likely influenced by wind and rain from foliar hosts to uninfested trees, but to fully understand the disease spread, it is necessary to examine the disease infection over broader spatial and temporal scales.

Earlier, Kelly and Meentemeyer (2002) presented a landscape approach to examining the spatial–temporal patterns of oak mortality in a relatively small area over 2 years. This paper takes further steps to characterize and model the spatial–temporal patterns of oak mortality at a larger spatial extent and across a longer temporal frame and examines explicitly the spatial association between dead trees and one important foliar host—California bay. Specifically, we consider two types of spatial point pattern analyses in order to characterize and model the spatial–temporal variability of mortality patterns associated with SOD. The first type of analysis, referred to as univariate spatial point pattern analysis, considers the interaction or dependence among points in a single spatial point pattern of oak mortality at a particular time period. The second type of analysis, referred to as multivariate spatial point pattern analysis, considers the spatial–temporal interaction among points in multiple spatial point patterns of oak mortality across different time frames and the interaction between dead oak trees and their foliar host—California bay.

2. Study area

The study area is located at the China Camp State Park (CCSP) in Marin County, California. This area has been a hotspot for SOD research as it displays extensive overstory mortality of coast live oaks and black oaks (Rizzo and Garbelotto, 2003; Kelly et al., 2004a,b; McPherson et al., 2005). The park is about 600 ha in size, with elevations ranging from sea level at San Francisco Bay to 290 m. Average slopes in the park are around 30–40%, and extreme slopes can approach 100%. Vegetation in the park is varied but is dominated by mixed hardwood forest. Coast live (*Quercus agrifolia*), black (*Quercus kelloggii*) and valley oaks (*Quercus lobata*) are common, and occur with mature madrone (*Arbutus menziesii*) and California bay (*Umbellularia californica*) trees. The understory is comprised of shrubs and small trees and vines, including manzanita, (*Arctostaphylos manzanita*), toyon (*Heteromeles arbutifolia*), hazel (*Corylus cornuta*), and buckeye (*Aesculus californica*). All of these plants with the exception of valley oak are hosts for *P. ramorum* (McPherson et al., 2005; www.suddenoakdeath.org).

3. Methods

3.1. Remote sensing data and mapped point patterns

Multi-temporal high spatial resolution airborne images, ADAR 5500 (Airborne Data Acquisition and Registration), acquired in 2000, 2001, 2002, and 2003 were used as the primary source to derive mapped point data for further spatial point pattern analyses. The average ground spatial resolution of the ADAR images is 1 m, which permits sufficient spatial details for mapping individual dead crowns from the imagery. Liu et al. (2006) developed a new spatial–temporal classification algorithm using the first 2 years' ADAR images for mortality mapping and generated very accurate classification results (about 95%). In this study, we applied the same classification algorithm to the multi-temporal ADAR images to map the SOD mortality over 4 years.

The spatial point patterns of mortality were generated from the four classified images in the following three steps: firstly, neighboring pixels classified as dead trees were aggregated to objects for each classified image; secondly, objects that are too small or irregular (Guo et al., 2007) to be dead crowns are removed in order to eliminate pseudo dead trees due to classification errors; thirdly, the centroid of each object was derived as the final point location of the dead tree. Because dead trees can remain more than 1 year if not removed, some dead trees derived from one image may also exist on the later images. To create multi-temporal point patterns of mortality marked by time, the points which have been recorded in all the previous spatial point patterns were eliminated from each present point pattern so that each point pattern only contained newly dead trees since the last image acquisition. The four mapped spatial point patterns of oak mortality are shown in Fig. 1, where the numbers of dead trees are 4614 in 2000, 1213 in 2001, 247 in 2002, and 191 in 2003. The exploratory analysis of the first order intensity using kernel smoothing with bandwidth of 400 m estimated the corresponding intensity maps in Fig. 1, indicating the presence of a large scale trend from northeast to southwest in all the mapped spatial point patterns.

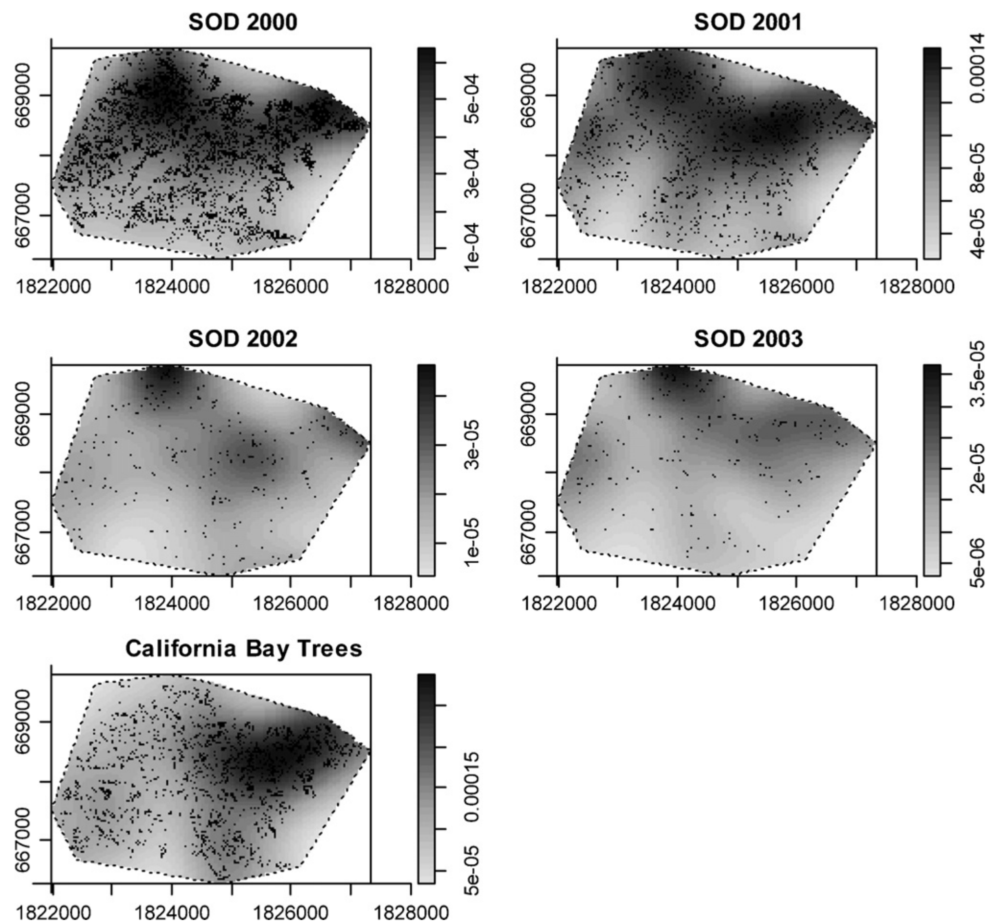

Fig. 1. Mapped spatial point patterns and the estimated intensities.

To investigate the spatial relationship between oak mortality and its major foliar hosts, we mapped point patterns of one major type of overstory foliar host, California bay (*Umbellularia californica*), by digitizing points on the ADAR imagery of year 2001 based on field experience and data used in a previous study (Kelly and Meentemeyer, 2002). This generated 1814 bay trees in the study area. Other types of foliar hosts are not considered here because they are mainly understory and hard to map from the remotely sensed imagery. The spatial point pattern for bay trees and its intensity map are shown in Fig. 1. Similarly, a spatial trend can be identified from the map.

3.2. Univariate spatial point pattern analysis

3.2.1. Characterizing SOD point patterns by K-functions

Ripley's *K*-function (Ripley, 1977) is a powerful technique for assessing within-pattern point interactions at multiple scales through the analysis of a wide range of within-pattern point distances. It has been used in various forest spatial pattern analyses (Diggle, 1983; Cressie, 1991; Penttinen et al., 1992; Moeur, 1993; Haase, 1995; Vacek and Leps, 1996; Kelly and Meentemeyer, 2002).

Consider a stationary point process $S = \{s_1,\ldots,s_n\}$ with constant intensity λ, *K*-function $K(h)$ is defined such that $\lambda K(h)$ equals the expected number of random points within a distance of h to an arbitrary point in the process S and is estimated as:

$$\hat{K}(h) = \frac{1}{|\Re|}\sum_{i=1}^{n}\sum_{j\neq i}\frac{w_{ij}I(d_{ij}\leq h)}{\lambda^2} \tag{1}$$

where $|\Re|$ denotes the area of study region $\Re$; d_{ij} is the distance between point s_i and point s_j; $I(d_{ij} \leq h)$ equals to 1 if $d_{ij} \leq h$ and 0 otherwise; w_{ij} is an edge-correction term to remove the bias introduced by the edge of $\Re$ (Ripley, 1977); the intensity λ can be estimated by $\hat{\lambda} = n/|\Re|$. *K*-function makes the assumption of stationarity and isotropic point process, so it is frequently used as a valid second order statistic to test for the null hypothesis of complete spatial randomness (CSR), under which a point process is assumed as a homogeneous Poisson process (HPP). However, the assumption of stationarity may not hold due to the existence of hidden spatial covariates to the intensity function (Stoyan and Stoyan, 1994; Berndtsson, 1989; Brodie et al., 1995; Wu et al., 2000). Under such circumstances, the interpretation of *K*-function can be misleading because any spatial dependence or departure from CSR could be a result of small scale variation of the intensity of an inhomogeneous point process rather than within-pattern point interaction. As all the mapped SOD point patterns exhibit spatial trends, they are non-stationary patterns and it is necessary to consider the spatial trend effects when testing the hypothesis on second order spatial dependencies. To do this, we used in this paper a relatively new technique, inhomogeneous K-function (Baddeley et al., 2000) with our mapped point patterns. The inhomogeneous K-function denoted by K_{inhom} is a generalization of Ripley's K-function to an inhomogeneous point process where second-order intensity-reweighted stationarity is assumed (Baddeley et al., 2000). As a non-stationary analogy of K-function, K_{inhom} is used to examine the spatial dependence of a point pattern with non-constant intensities by adjusting the spatial heterogeneity of the point pattern. Given a non-stationary spatial process $S = \{s_1, \ldots, s_n\}$ with spatially varying intensity function $\lambda(s)$, the inhomogeneous K-function is estimated as:

$$\hat{K}_{\text{inhom}}(h) = \frac{1}{|\Re|}\sum_{i=1}^{n}\sum_{j \neq i}\frac{w_{ij}I(d_{ij} \leq h)}{\lambda(s_i)\lambda(s_j)}, \tag{2}$$

where $\lambda(s_i)$ and $\lambda(s_j)$ are the values of the intensity function $\lambda(s)$ at point s_i and point s_j, respectively. Specifically, the intensity function $\lambda(s)$ was modeled as a log linear function of spatial coordinates:

$$\lambda(s) = \exp(\beta^T X(s)), \tag{3}$$

where $X(s)$ is a vector of polynomials of Cartesian coordinates x, y of point s. The model fitting can be solved using maximum pseudo-likelihood methods (Besag, 1975).

To assess the strength of the within-pattern point interactions of the non-stationary SOD point patterns, we generalized the simple HPP under the standard CSR assumption to a more realistic inhomogeneous Poisson process (IPP) (Diggle, 1983), and tested the mapped point patterns with the null hypothesis of IPP using the inhomogeneous K-function and Monte Carlo simulations. To detect the departure from IPP, we constructed 99% confidence envelopes of IPP characterized by the estimated intensity function by 99 Monte Carlo simulations in the following two steps (Diggle, 1983):

(1) Randomly generate HPP over the region of mapped points, $\Re$, with maximum intensity of the study area: $\lambda_{\max} = \sup_{s \in \Re}[\lambda(s)]$;
(2) Stochastically thin the simulated HPP (s_1, $s_2, \ldots, s_n$) by removing the generated points $s_i (i = 1,2,\ldots,n)$ with probability $1 - \lambda(s_i)/\lambda_{\max}$.

3.2.2. Modeling SOD point patterns by Neyman–Scott processes

The estimates of K-function (or inhomogeneous K-function) together with the confidence envelopes constructed from Monte Carlo simulation of HPP (or IPP) can only assess the strength of interaction or dependence between points against Poisson models. When point patterns significantly depart from Poisson processes, alternative stochastic processes should be developed to model the interactions within point patterns. Neyman–Scott processes represent a large class of stochastic models for spatial clustering. As aggregation dominates the spatial patterns of oak mortality, we modeled the aggregated SOD point patterns as Neyman–Scott processes (Diggle, 1983; Cressie, 1991). Specifically, the Neyman–Scott processes considered in this paper are based on the following definition:

1. Parent events C are generated by a HPP with intensity ρ.
2. Each parent $c \in C$ independently produces a random number S of offspring Y_c, where S follows a Poisson distribution with mean μ.
3. The offspring events Y_c are distributed relative to their parent c according to a bivariate Gaussian density function with mean $\mathbf{0}$ and variance matrix $\sigma^2\mathbf{I}$.
4. The final process is composed of the superposition of the offspring only (i.e. $Y = \cup_{c \in C} Y_c$).

The above definition essentially determines a homogeneous Neyman–Scott process (HNSP) because the parent events are HPP and the offspring events are radically symmetric about $\mathbf{0}$ (Cressie, 1991). It is easy to show that the constant intensity function of the HNSP Y is $\lambda_Y = \rho\mu$. The theoretical K-function of the HNSP is

$$K_{\text{HNSP}}(h, \sigma, \rho) = \pi h^2 + \frac{1 - \exp(-h^2/4\sigma^2)}{\rho}. \tag{4}$$

Given a user-specified maximum distance h_0, the model parameters for Y can be estimated by minimizing the "discrepancy measure" $D(\sigma,\rho)$ of the empirical K-function $\hat{K}(h)$ of Y and the expected value $K_{\text{HNSP}}(h,\sigma,\rho)$ (Diggle, 1983):

$$D(\sigma, \rho) = \int_0^{h_0} (\hat{K}(h)^{0.25} - K_{\text{HNSP}}(h, \sigma, \rho)^{0.25})^2 \mathrm{d}h. \tag{5}$$

To account for the non-stationarity of the mapped oak mortality patterns, we further modeled the SOD point patterns as inhomogeneous Neyman–Scott processes (INSP) (Waagepetersen, 2007). The inhomogeneous Neyman–Scott process X can be thought of as a thinned process of the homogeneous Neyman–Scott process Y (Waagepetersen, 2007), where the spatially varying thinning probability $f(s)$ is related to the spatially varying intensity function $\lambda(s)$ in (3) as $f(s) = \lambda(s)/\max\{\lambda(s)\}$. Accordingly, the intensity function of the INSP is $\lambda_X(s) = \lambda_Y(s)f(s)$. Since the mapped oak mortality patterns are non-stationary, they should be regarded as X. We are interested in the model parameters of the hidden HNSP Y which generates the observed INSP X. As the inhomogeneous K-function for X coincides with the K-function for Y (Baddeley et al., 2000; Waagepetersen, 2007), the model parameters of the underlying HNSP Y can be estimated by minimizing the "discrepancy measure" $D(\sigma,\rho)$ of the empirical inhomogeneous K-function $\hat{K}_{\text{inhom}}(h)$ of X and the expected value $K_{\text{HNSP}}(h,\sigma,\rho)$ (Waagepetersen, 2007):

$$D(\sigma, \rho) = \int_0^{h_0} (\hat{K}_{\text{inhom}}(h)^{0.25} - K_{\text{HNSP}}(h, \sigma, \rho)^{0.25})^2 \mathrm{d}h. \tag{6}$$

3.3. Multivariate spatial point pattern analysis

A multivariate spatial point pattern refers to a point pattern consisting of two or more types of points, which are characterized by different marks. In this paper, we consider two types of multivariate spatial point pattern interactions: (1) the multivariate point patterns marked by time; specifically, the interaction of SOD point patterns through time, and (2) the multivariate point patterns marked by tree species; specifically, the interaction between the SOD point patterns and the point pattern of one major foliar host, California bay trees.

The spatial dependence between point patterns in a multivariate point process is related to the second order properties of the multivariate spatial point process, which can be defined by cross second-moment measures (Cressie, 1991). A direct generalization of Ripley's *K*-function to a multivariate point process is the reduced cross-second moment measure (Hanisch and Stoyan, 1979), called the cross-*K*-function. Given a stationary multivariate spatial point process where the intensity of the sub-process marked as i is λ_i, the cross-*K*-function $K(i, j; h)$ is defined so that $\lambda_j K(i, j; h)$ equals the expected number of random points of sub-process j within a distance h of an arbitrary point of sub-process i. As is the case for the *K*-function in univariate spatial point pattern analysis, the cross-*K*-function may not be applicable to a multivariate spatial point process where any one of the sub-processes is not stationary. The between-pattern point interaction could be a result of the spatial variation of a sub-process point intensity function. To account for the spatial trends in the mapped point patterns, we investigated the inhomogeneous version of the cross-*K*-function, called inhomogeneous cross-*K*-function (Møller and Waagepetersen, 2004). The inhomogeneous cross-*K*-function is formulated to adjust the spatially varying intensity of a non-stationary multivariate point process in a similar way as the adjustment of the inhomogeneous *K*-function to Ripley's *K*-function. Consider a non-stationary multivariate spatial point process consisting of p sub-processes, denoted by:

$$S = \{S_1, \ldots, S_p\} = \{\{s_{11}, \ldots, s_{1N_1}\}, \ldots, \{s_{p1}, \ldots, s_{pN_p}\}\}, \tag{7}$$

with spatially varying intensity function $\lambda_i(s)$ for sub-process i, the inhomogeneous cross-*K*-function between sub-process S_m and sub-process S_n is estimated as:

$$\hat{K}_{\text{inhom}}(m, n; h) = \frac{1}{|\Re|} \sum_{i=1}^{N_m} \sum_{j=1}^{N_n} \frac{w_{ij} I(d_{ij} \le h)}{\lambda_m(s_{m,i}) \lambda_n(s_{n,j})}, \tag{8}$$

where N_m, N_n are the total numbers of points for sub-processes S_m and S_n, respectively; d_{ij} is the distance between point $s_{m,i}$ in sub-process S_m and point $s_{n,j}$ in sub-process S_n.

Formal assessment of the interaction between non-stationary multivariate spatial point patterns can be developed by calculating the inhomogeneous cross-*K*-function and testing the null hypothesis that the multivariate point patterns are spatially independent. To detect the departure from independence, the 99% confidence envelopes of independence can be constructed by 99 Monte Carlo simulations of independent non-stationary multivariate point patterns. In doing so, we investigated two approaches to simulating independent non-stationary multivariate point patterns: a direct approach and an indirect approach. The direct approach assumes that the marginal distribution of the sub-processes can be modeled as INSP. Thus, it simulates the joint realization of independent non-stationary multivariate point patterns by independently generating sub-processes from the modeled INSP (see Section 3.2.2). The effectiveness of this approach relies on the goodness-of-fit of the models.

When the exact models of the sub-processes are unknown, an indirect approach can be developed to simulate independent point patterns. "Random toroidal shifting" (Lotwick and Silverman, 1982) is such an indirect approach to simulating independence between mulivariate point patterns. This approach randomly shifts one sub-process with respect to the other within a torus area wrapped by a rectangular region $\Re$, where points shifted out of $\Re$ will reappear to a new position in $\Re$ from the opposite side (Smith, 2004). However, the "random toroidal shifting" is not applicable to non-stationary multivariate spatial point processes because it assumes that the underlying sub-processes are stationary. To account for the non-stationarity of our mapped point patterns, we developed a new indirect approach to simulating independent realizations of non-stationary multivariate point patterns. The new approach, denoted as "random rotating", does not require stationarity. It generates independent point patterns by randomly rotating one sub-process with respect to its centroid whereas keeping another sub-process fixed. The random rotation is implemented in the two steps: (1) approximate the original study region $\Re$ using a circular region $\Re_c$ centered on the centroid of $\Re$, and (2) randomly rotate one sub-process with respect to the centroid.

4. Results

4.1. Univariate spatial point pattern analysis

4.1.1. Characterizing SOD point patterns by K-functions

The Ripley's *K*-functions assuming HPP were first calculated for each of the four SOD point patterns to demonstrate the influence of spatial trend when testing for the within-pattern point interactions. The empirical *K*-functions and the 99% confidence envelops of the simulated HPP are plotted against distances in Fig. 2. Linear transformations ($L(h) = \sqrt{K(h)/\pi} - h$) are applied to all *K*-functions for visualization purposes. For point patterns in 2000 and 2001, the transformed empirical *K*-functions keep increasing with distance and significantly exceed the upper bound at all distances, indicating strong spatial trends at large scales. For point patterns in 2002 and 2003, the transformed empirical *K*-functions level off at larger distances but still significantly exceed the upper bound at all distances, indicating less strong spatial trends at large scales compared to the first 2 years.

The spatial trends were accounted for by the non-stationary intensity functions $\lambda(s)$ which were estimated as log linear functions of second order polynomials of Cartesian coordinates x, y of location s after model selection. The model parameters listed in Table 1 were estimated using the R package called *spatstat* (Baddeley and Turner, 2005). The inhomogeneous *K*-functions were then calculated based on the estimated non-stationary intensity functions. The empirical inhomogeneous

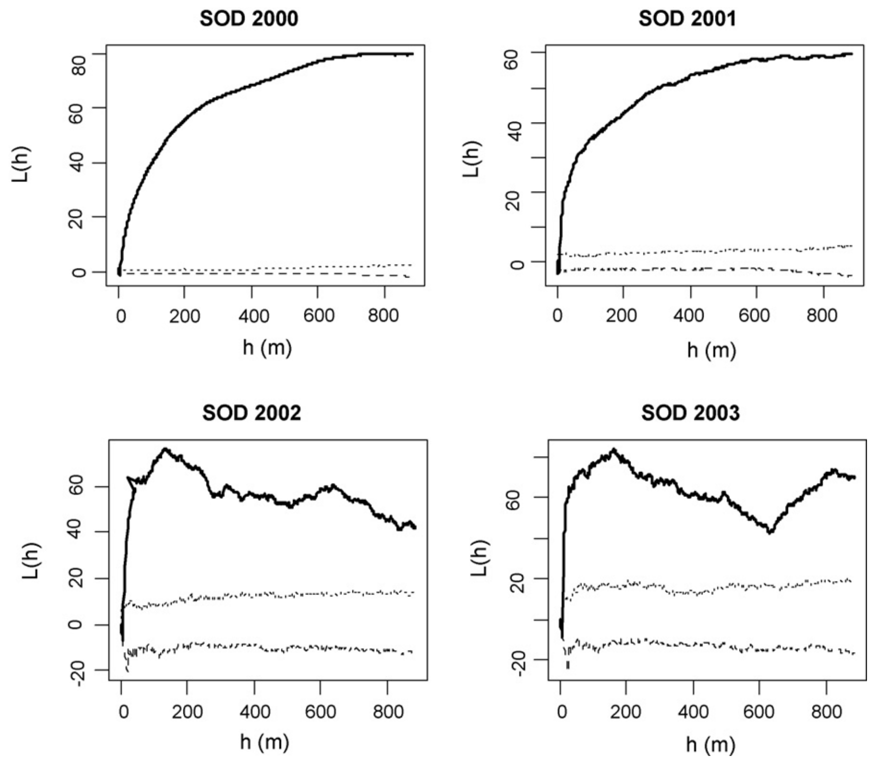

Fig. 2. *K*-functions of the SOD point patterns assuming HPP. The solid thick lines represent the empirical values of $L(h)$ (=$\sqrt{K(h)/\pi} - h$) and the dotted (dashed) lines represent the upper (lower) bounds of the 99% confidence envelops constructed with 99 Monte Carlo simulations of the fitted HPP.

K-functions and the 99% confidence envelopes of the simulated IPP are plotted against distances in Fig. 3. Linear transformations ($L(h) = \sqrt{K_{\text{inhom}}(h)/\pi} - h$) are applied to all inhomogeneous *K*-functions. The difference between the *K*-functions in Fig. 2 and the inhomogeneous *K*-functions in Fig. 3 indicates the influence of spatial trends in the estimation of second-order statistic. For all the point patterns in Fig. 3, the transformed empirical inhomogeneous *K*-function significantly exceeds the upper bound up to certain extent, indicating strong within-pattern point dependence or clustering with respect to non-stationary point process. The extent of clustering, determined as the maximum distance beyond which empirical $L(h)$ fall into the 99% confidence bounds of IPP, varies across the 4 years as follows: (1) up to 700 m in 2000, (2) up to 550 m in 2001, (3) up to 380 m in 2002, and (4) up to 350 m in 2003. The scale of the dominant clustering, determined as the distance $h_{\max}$ corresponding to the peak value of all $L(h)$, varies across the four point patterns as follows: (1) 200 m in 2000, (2) 160 m in 2001, (3) 80 m in 2002, and (4) 60 m in 2003. The variations of the extent and dominant scale of clustering among 4 years present some interesting findings: (1) both the extent and the scale decrease with time, and (2) both values in 2000 and 2001 are significantly larger than those in 2002 and 2003. This may indicate a possible disease progression from disease establishment to disease spread. Given our 4-year observations, a dividing point can be drawn between the first 2 years and the second 2 years: the early stage (before summer of 2001) of disease development is mainly focused on the initial disease establishment which is characterized by larger extent and scale of mortality clustering; the later stage (after summer of 2001) of disease development is shifted to disease spread from the established mortality which is characterized by decreased spatial extent and scale of clustering. McPherson et al. (2005) found that survival time for *Q. agrifolia* declined rapidly with disease severity, from 29 to 2.7 years, thus we think we might have a time-span sufficient to capture spread. We also acknowledge that we might be seeing difference in disease expression across the park.

4.1.2. Modeling SOD point patterns by Neyman–Scott processes

For comparison purposes, we present the results for both HNSP and INSP fitted to the mapped oak mortality patterns.

Table 1
Model parameters of the SOD point patterns assuming Poisson process (the model: $\lambda(s) = \exp(\beta_0 + \beta_1 x + \beta_2 y + \beta_3 x^2 + \beta_4 xy + \beta_5 y^2)$)

	$\hat{\beta}_0$	$\hat{\beta}_1$	$\hat{\beta}_2$	$\hat{\beta}_3$	$\hat{\beta}_4$	$\hat{\beta}_5$
2000	−4.75e5	3.27e−1	5.29e−1	−1.02e−7	6.82e−8	−4.89e−7
2001	−4.53e5	3.18e−1	4.90e−1	−8.42e−8	−1.53e−8	−3.45e−7
2002	−3.17e5	2.36e−1	3.03e−1	−5.24e−8	−6.63e−8	−1.36e−7
2003	−1.21e5	1.14e−1	5.17e−2	−4.82e−8	9.32e−8	−1.66e−7

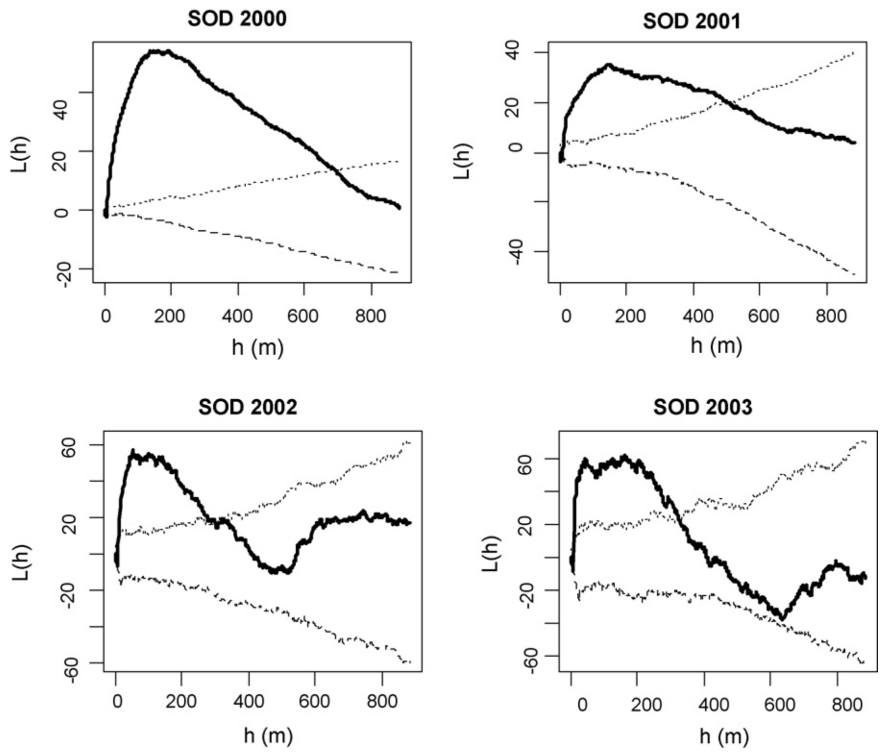

Fig. 3. *K*-functions of the SOD point patterns assuming IPP. The solid thick lines represent the empirical values of $L(h)$ $(=\sqrt{K_{\mathrm{inhom}}(h)/\pi} - h)$ and the dotted (dashed) lines represent the upper (lower) bounds of the 99% confidence envelops constructed with 99 Monte Carlo simulations of the fitted IPP.

The model parameters estimated by *spatstat* are listed in Tables 2 and 3. The interpretations of the model parameters in the two tables are slightly different: the parameters in Table 2 correspond to the fitted HNSP under the assumption that the mapped SOD point patterns are HNSP; in contrast, the parameters in Table 3 correspond to the fitted hidden HNSP under the assumption that the mapped SOD point patterns are INSP generated by thinning the hidden HNSP. The minimized ‘‘discrepancy measures’’ $D(\hat{\sigma}, \hat{\rho})$ in Table 3 are much smaller than those in Table 2 for the four point patterns, indicating that INSP are better fits to the mapped mortality patterns. This result reflects the influence of spatial trends as showed in the *K*-function analysis in Section 4.1.1. We hereby only discuss the model parameters in Table 3. The estimated intensity $\hat{\rho}$ of the parent events in the hidden HNSP increases from 2000 to 2003. This is equivalent to the increase in the number of clusters from 2000 to 2003, indicating the decreasing aggregations over time. The estimated displacement parameter $\hat{\sigma}$ decreases from 2000 to 2003. As σ determines the spatial dispersion of the offspring, it is proportional to the cluster size. Therefore, the decreasing σ indicates that the cluster size of the mortality pattern decreases with time. Moreover, the contrast of σ between the first 2 years and the last 2 years is noticeable. These results are consistent with those showed in Fig. 3. Comparatively, the model fitting in 2003 is not as good as other years because the minimized ‘‘discrepancy measure’’ in 2003 is much larger than the other years.

The empirical *K*-functions (or inhomogeneous *K*-functions), the fitted *K*-functions, and the 99% confidence envelopes constructed by 99 simulations of fitted HNSP (or fitted hidden HNSP) are plotted against distances in Fig. 4 (or Fig. 5). For all the point patterns in Figs. 4 and 5, nearly all the transformed empirical values fall well within the 99% confidence envelopes. However, the differences between the empirical values and fitted values are smaller in Fig. 5 than those in Fig. 4 for all years, which are indicated by the smaller minimized ‘‘discrepancy measures’’ in Table 3 than in Table 2. Similarly, there is a large difference between the empirical values and fitted values in 2003 as indicated by its larger minimized ‘‘discrepancy measure’’.

Table 2
Model parameters of the SOD point patterns assuming HNSP

	2000	2001	2002	2003
$\hat{\rho}$	2.9e−6	4.3e−6	7.6e−6	6.9e−6
$\hat{\sigma}$	197.1	172.2	57.9	54.2
$D(\hat{\sigma}, \hat{\rho})$	67.2	102.5	211.4	353.6

Table 3
Model parameters of the SOD point patterns assuming INSP

	2000	2001	2002	2003
$\hat{\rho}$	5.5e−6	1.1e−5	1.5e−5	1.7e−5
$\hat{\sigma}$	108.2	81.7	39.8	31.6
$D(\hat{\sigma}, \hat{\rho})$	43.7	53.8	92.9	200.9

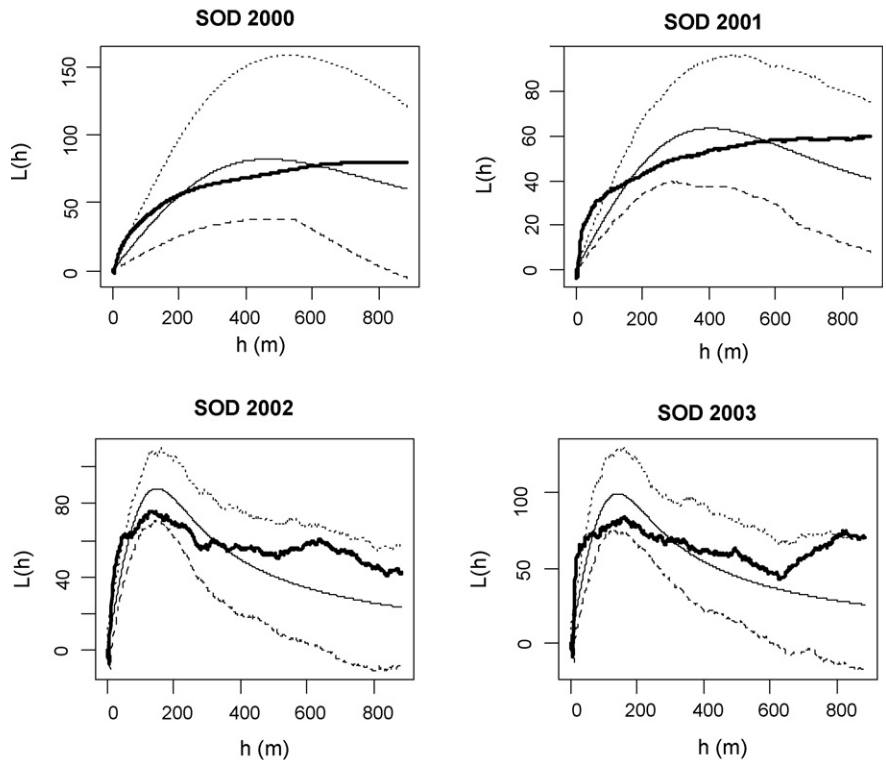

Fig. 4. *K*-functions of the SOD point patterns assuming HNSP. The solid thick lines represent the empirical values of $L(h)$ $(=\sqrt{K(h)/\pi}-h)$; the solid lines represent the fitted values of the HNSP; and the dotted (dashed) lines represent the upper (lower) bounds of the 99% confidence envelops constructed with 99 Monte Carlo simulations of the fitted HNSP.

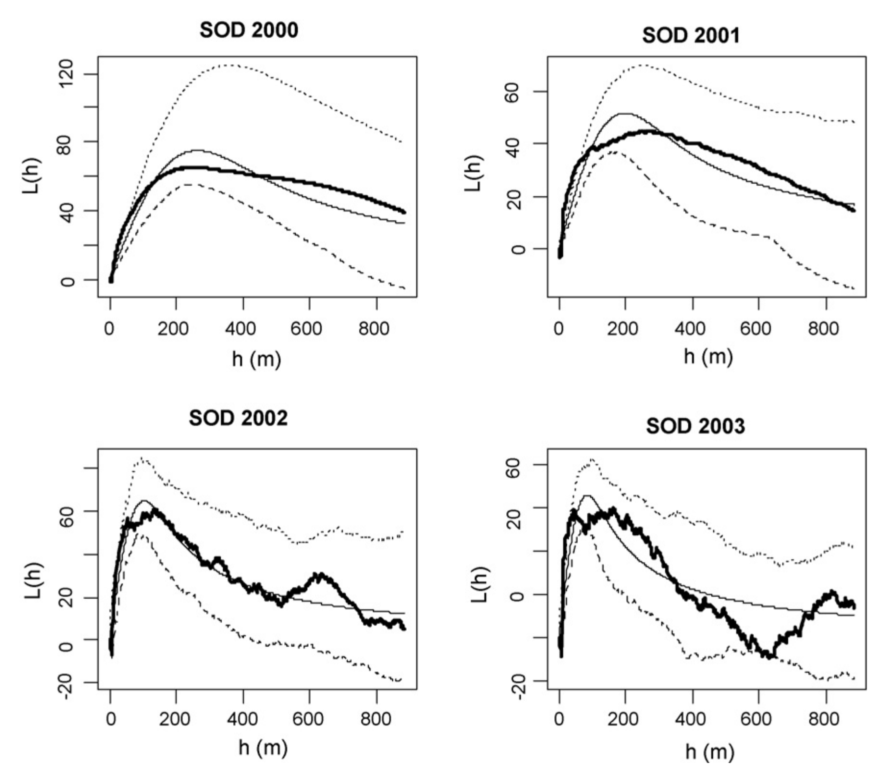

Fig. 5. *K*-functions of the SOD point patterns assuming INSP. The solid thick lines represent the empirical values of $L(h)$ $(=\sqrt{K_{\text{inhom}}(h)/\pi}-h)$; the solid lines represent the fitted values of the INSP; and the dotted (dashed) lines represent the upper (lower) bounds of the 99% confidence envelops constructed with 99 Monte Carlo simulations of the fitted INSP.

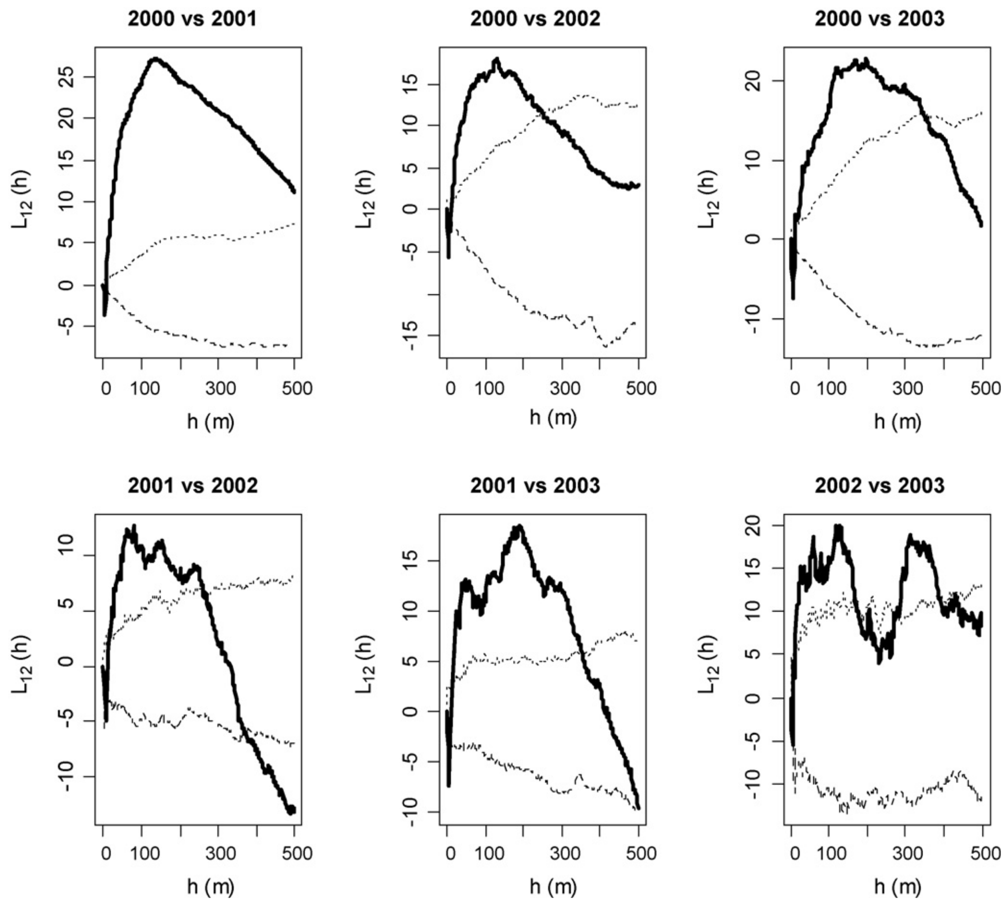

Fig. 6. Inhomogeneous cross-K-functions of all pairwise SOD point patterns. The solid thick lines represent the empirical values of $L_{12}(h)$ $(=\sqrt{K_{\text{inhom}}(1,2,h)/\pi}-h)$ and the dotted (dashed) lines represent the upper (lower) bounds of the 99% confidence envelops constructed with 99 Monte Carlo simulations of independent joint point processes using the fitted INSP.

4.2. Multivariate spatial point pattern analysis

4.2.1. Independence test among SOD point patterns across time

The inhomogeneous cross-K-functions of pairwise SOD point patterns were calculated based on the non-stationary intensity functions estimated in Section 4.1.1. In Figs. 6 and 7, the empirical inhomogeneous K-functions and the 99% confidence envelopes are plotted against distances. The confidence envelopes were constructed with 99 Monte Carlo simulations of independent joint point processes using the fitted INSP in Fig. 6 and using the proposed "random rotating" method in Fig. 7. Linear transformations $(L_{12}(h)=\sqrt{K_{\text{inhom}}(1,2;h)/\pi}-h)$ are applied to all inhomogeneous cross-K-functions. The results from Figs. 6 and 7 are consistent in the relationships between the empirical inhomogeneous K-functions and the 99% confidence envelopes except that the confidence envelopes in Fig. 6 are narrower than those in Fig. 7. Both figures show that the transformed empirical cross-inhomogeneous K-functions of all pairwise point patterns significantly exceed the 99% upper bound, indicating strong evidence of between-pattern point dependence (i.e. attraction). The scales of the dependence, determined as the distance at which the peak values of all $L_{12}(h)$ are achieved, vary among different pairwise point patterns: (1) the attractions between 2000 and the later 3 years (2001, 2002, and 2003) are approximately at the scale of 150 m, and (2) the attractions among the later 3 years have multiple scales ranging from 100 to 300 m. The strong dependence between earlier years and later years indicates that new dead oak trees tend to locate within up to 300 m to past dead oak trees. This positive dependence may indicate that the environmental niche of the pathogen is spatially varied in a similar way at different time of disease development.

4.2.2. Independence test between SOD and California bay trees

The inhomogeneous cross-K-functions between SOD and the foliar host, California bay trees, were calculated based on the stack of 4 years' SOD point patterns and the bay tree point pattern. The plots of the empirical inhomogeneous K-functions and the 99% confidence envelopes against distances are shown in Fig. 8. The confidence envelopes were constructed with 99 Monte Carlo simulations of independent joint point processes using the fitted INSP in Fig. 8(a) and the proposed "random rotating" method in Fig. 8(b). The results showed that strong attraction existed between SOD mortality and California bay trees, in which the transformed empirical inhomogeneous

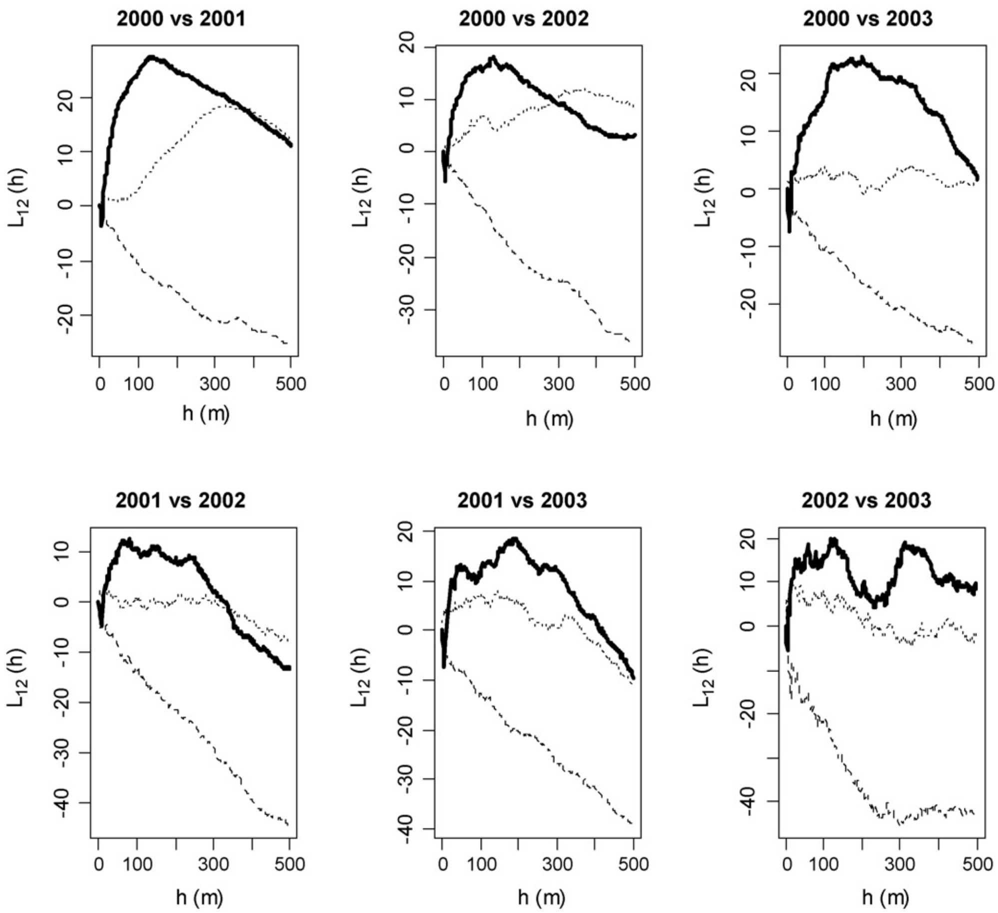

Fig. 7. Inhomogeneous cross-*K*-functions of all pairwise SOD point patterns. The solid thick lines represent the empirical values of $L_{12}(h)$ ($=\sqrt{K_{\mathrm{inhom}}(1,2,h)/\pi}-h$) and the dotted (dashed) lines represent the upper (lower) bounds of the 99% confidence envelops constructed with 99 Monte Carlo simulations of independent joint point processes using ‘‘random rotating’’.

cross-*K*-functions significantly lie above the 99% upper bound. The value of $L_{12}(h)$ is peaked around 150 m, indicating that the dominant scale of the dependence is at 150 m. The strong dependence between SOD and California bay trees indicates that SOD points tend to locate within 150 m of the bay tree points. This positive dependence may confirm that the presence of foliar hosts is contributing to the disease spread by serving as the medium for the pathogen over large spatial scales.

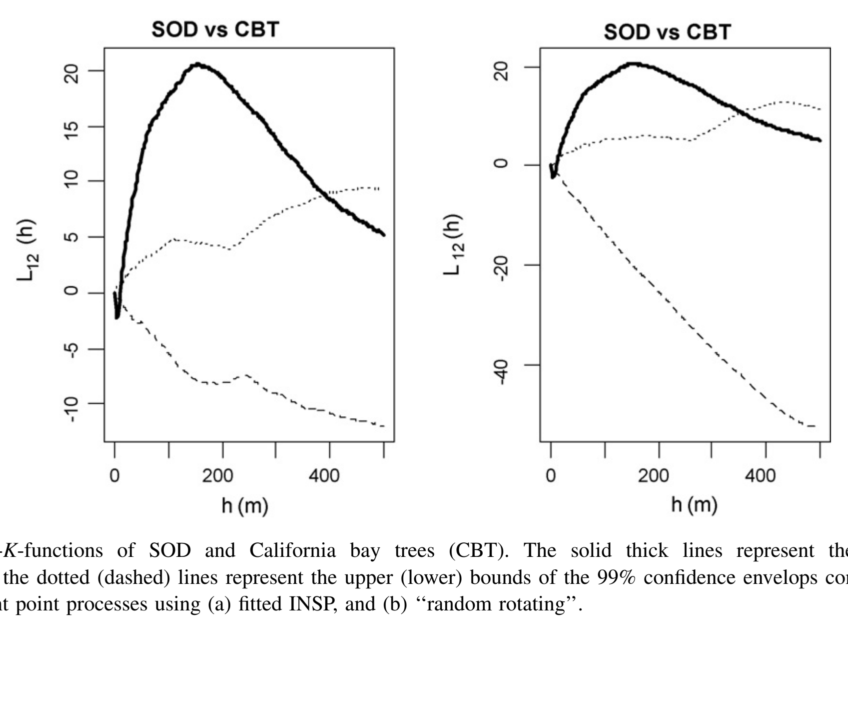

Fig. 8. Inhomogeneous cross-*K*-functions of SOD and California bay trees (CBT). The solid thick lines represent the empirical values of $L_{12}(h)$ ($=\sqrt{K_{\mathrm{inhom}}(1,2,h)/\pi}-h$) and the dotted (dashed) lines represent the upper (lower) bounds of the 99% confidence envelops constructed with 99 Monte Carlo simulations of independent joint point processes using (a) fitted INSP, and (b) ‘‘random rotating’’.

5. Discussion

5.1. Univariate point pattern analysis

In the univariate point pattern analysis, we examined the within-pattern point dependence of individual SOD point patterns using inhomogeneous *K*-functions in order to accommodate the spatial heterogeneity of the first order intensity. The spatial inhomogeneous distribution of the point intensity could be the result of the variation of population at risk, as is often the case in epidemiological studies. However, the forest in our study area is characterized by dense close canopy hardwood populated with oak species. It might be reasonable to assume a homogenous population of terminal hosts. Consequently, we could tackle this problem by estimating the non-stationary intensity functions of the inhomogeneous point patterns. In this study, we estimated the non-stationary intensity function prior to the calculation of the inhomogeneous *K*-function. This process separates the first-order and second-order structure explicitly, so the second-order analysis is dependent on the estimated intensity function. Both parametric and non-parametric methods can be used to estimate first-order intensity function. If a non-parametric method is used, one may assume that the scale of the first order structure is larger than that of the second order structure (Diggle et al., 2007). Otherwise, a parametric estimation method would be more appropriate. For simplicity, we estimated the intensity function using a parametric form of the spatial coordinates of each point. Specifically, the intensity function was modeled as a log linear polynomial function of spatial coordinates. It should be noted that this simple parametric form can only capture the general trend of the intensity function. If more covariates underlying the mortality process are incorporated into the model, the intensity estimation could be improved. Some candidate environmental covariates could be (1) topography related factors such as elevation, slope, radiation index, and moisture index and (2) forest species factors such as the terminal host and foliar host density.

5.2. Multivariate point pattern analysis

In the multivariate point pattern analysis, we examined spatial dependence of multivariate point patterns using inhomogeneous cross-*K*-functions in order to accommodate the spatial heterogeneity of the first order intensity. The main challenge in the hypothesis test of the dependence between different point patterns is to simulate sampling distribution of independent joint point processes given that the underlying spatial point processes are non-stationary and their distributions are unknown. Two simulation approaches developed in this paper have different perspectives in generating independent joint point processes. The first approach is a model-based approach. It directly simulates independent point patterns using random realizations of sub-processes modeled by Neyman–Scott processes. As a result, the point pattern generated in each simulation is different from the original pattern in number and structure. The second simulation approach, referred to as ''random rotating'', generalizes the conventional ''random toroidal shifting'' to cope with the spatial trend in the point patterns. This approach is more general as it does not require fitting models to point patterns. This approach uses rotating rather than shifting to keep the spatial structures of the original non-stationary point processes unchanged. In addition, the circular boundary is invariant to different random rotations. As a result, the point pattern generated in each simulation is the same as the original point pattern and the only difference is that it is randomly rotated. However, the circular boundary may be problematic when the study region has an elongated shape, which is hard to approximate using a circular boundary. Further research is needed to solve these problems.

6. Conclusions

In this study, we applied both univariate and multivariate spatial point pattern analysis methods to characterize and model the spatial–temporal variability of oak mortality using the point patterns mapped from remotely sensed images over time. The univariate point pattern analysis focuses on the first and second order structures of SOD point patterns at different years. The spatially varying first order point intensity functions were modeled as log linear polynomials of spatial coordinates. Then, the inhomogeneous *K*-functions were used to analyze the second order within-pattern point interactions. Monte Carlo methods were used to simulate IPP, from which the confidence envelopes were constructed to test the null hypothesis of IPP. The results showed that the SOD point patterns are significantly clustered at different scales and spatial extents through time, revealing that the underlying mortality process consists of first order trend and second order clustering rather than pure randomness. The decreasing extents and scales of clustering through time might indicate a possible transition from the early disease establishment to the later disease spread from the established mortality. Moreover, we investigated Neyman–Scott processes as alternative stochastic processes to IPP to model the aggregations of the SOD point patterns. The results indicated that inhomogeneous Neyman–Scott processes were good fits to the aggregated point patterns. The fitted Neyman–Scott models revealed that: (1) the aggregations were decreasing over time in terms of increased clusters; (2) the cluster size of the mortality pattern decreased with time; and (3) there was an obvious contrast in the cluster size between the first 2 years and the last 2 years. These observations are consistent with those from the results assuming IPP.

The multivariate point pattern analysis considers two types of dependence relationships between point patterns: (1) the spatial dependence within the multi-temporal SOD point patterns, and (2) the spatial dependence between SOD point patterns and their foliar host point pattern. Inhomogeneous cross-*K*-functions were applied to measure the between-pattern point interactions among different point patterns. To detect any evidence of dependence (positive or negative) from these point patterns, we developed two simulation approaches to generating sampling distribution of the independent joint point processes from which the confidence envelope under the null hypothesis of independence can be constructed. The results from the two approaches were similar and showed that there exist strong positive dependencies (i.e. attraction) within multi-temporal SOD point patterns through time, and importantly between SOD and California bay trees.

Acknowledgements

This work was supported by NASA Headquarters under the Earth System Science Fellowship Grant NGT5-30493 to D. Liu. The paper was strengthened with the comments of anonymous reviewers. The suggestions by Dr. Noel Cressie and Dr. Adrian Baddeley are appreciated.

References

Arevalo, J.R., Fernandez-Palacios, J.M., 2003. Spatial patterns of trees and juveniles in a laurel forest of tenerife, canary islands. Plant Ecol. 165, 1–10.

Baddeley, A., Møller, J., Waagepetersen, R., 2000. Non- and semi-parametric estimation of interaction in inhomogeneous point patterns. Stat. Neerlandica 54, 329–350.

Baddeley, A., Turner, R., 2005. Spatstat: an R package for analyzing spatial point patterns. J. Stat. Software 12, 1–42.

Batista, J.L.F., Maguire, D.A., 1998. Modeling the spatial structure of tropical forests. Forest Ecol. Manage. 110, 293–314.

Berndtsson, R., 1989. Topographical and coastal influence of spatial precipitation patterns in tunisia. Int. J. Climatol. 9, 357–369.

Besag, J., 1975. Statistical analysis of non-lattice data. The Statistician 24, 179–195.

Brodie, C., Houle, G., Fortin, M.J., 1995. Development of a populus balsamifera clone in subarctic quebec reconstructed from spatial analyses. J. Ecol. 83, 309–320.

Cole, R.G., Syms, C., 1999. Using spatial pattern analysis to distinguish causes of mortality: an example from kelp in north-eastern New Zealand. J. Ecol. 87, 963–972.

Cressie, N., 1991. Statistics for Spatial Data. Wiley, New York.

Dale, M.R.T., 1999. Spatial Pattern Analysis in Plant Ecology. Cambridge University Press, Cambridge, United Kingdom.

Davidson, J.M., Wickland, A.C., Patterson, H., Falk, K., Rizzo, D.M., 2005. Transmission of *Phytophthora ramorum* in mixed-evergreen forests in California. Phytopathology 95 (5), 587–596.

Davidson, J.M., Rizzo, D.M., Garbelotto, M., Tjosvold, S., Slaughter, G.W., 2002. Phytophthora ramorum and sudden oak death is California. II.In: Transmission and survival, *Fifth Symposium on Oak Woodlands*, USDA-Forest Service, San Diego, CA.

Diggle, P.J., 1983. Statistical Analysis of Spatial Point Patterns. Academic Press, London.

Diggle, P.J., Gómez-Rubio, V., Brown, P.E., Chetwynd, A.G., Gooding, S., 2007. Second-order analysis of inhomogeneous spatial point processes using case-control data. Biometrics 63, 550–557.

Franklin, J., Michaelsen, J., Strahler, A.H., 1985. Spatial analysis of density dependent patterns in coniferous forest stands. Vegetation 64, 29–36.

Goreaud, F., Loreau, M., Millier, C., 2002. Spatial structure and the survival of an inferior competitor: a theoretical model of neighbourhood competition in plants. Ecol. Model. 158, 1–19.

Guo, Q., Kelly, M., Gong, P., Liu, D., 2007. An object-based classification approach in mapping tree mortality using high spatial resolution imagery. GISci. Remote Sens. 44, 24–47.

Haase, P., 1995. Spatial pattern analysis in ecology based on Ripley's K-function: introduction and methods of edge correction. J. Vegetation Sci. 6, 575–582.

Hanisch, K.H., Stoyan, D., 1979. Formulas for second-order analysis of marked point processes. Math. Operationsforschung Stat. Ser. Stat. 10, 555–560.

Holdenrieder, O., Pautasso, M., Weisberg, P., Lonsdale, D., 2004. Tree diseases and landscape processes: the challenge of landscape pathology. Trends Ecol. Evol. 19, 446–452.

Kelly, M., Meentemeyer, R.K., 2002. Landscape dynamics of the spread of Sudden Oak Death. Photogrammetric Eng. Remote Sens. 68 (10), 1001–1009.

Kelly, M., Shaari, D., Guo, Q., Liu, D., 2004a. A comparison of standard and hybrid classifier methods for mapping hardwood mortality in areas affected by ''sudden oak death''. Photogrammetric Eng. Remote Sens. 70, 1229–1239.

Kelly, M., Tuxen, K., Kearns, F., 2004b. Geospatial informatics for management of a new forest disease: sudden oak death. Photogrammetric Eng. Remote Sens. 70, 1001–1004.

Liu, D., Kelly, M., Gong, P., 2006. A spatial–temporal approach to monitoring forest disease spread using multi-temporal high spatial resolution imagery. Remote Sens. Environ. 101 (2), 167–180.

Lotwick, H.W., Silverman, B.W., 1982. Methods for analyzing spatial processes of several types of points. J. R. Stat. Soc. B 44, 406–413.

McPherson, B.A., Mori, S.R., Wood, D.L., Storer, A.J., Svihra, P., Kelly, N.M., Standiford, R.B., 2005. Sudden oak death in California: disease progression in oaks and tanoaks. Forest Ecol. Manage. 213, 71–89.

Moeur, M., 1993. Characterizing spatial patterns of trees using stem-mapped data. Forest Sci. 39 (4), 756–775.

Møller, J., Waagepetersen, R.P., 2004. Statistical Inference and Simulation for Spatial Point Processes. Chapman and Hall, London.

Penttinen, A., Stoyan, D., Henttonen, H.M., 1992. Marked point process in forest statistics. Forest Sci. 38 (4), 806–824.

Ristaino, J.B., Gumpertz, M., 2000. New frontiers in the study of dispersal and spatial analysis of epidemics caused by species in the genus phyophthora. Annu. Rev. Phytopathol. 38, 541–576.

Rizzo, D., Garbelotto, M., 2003. Sudden oak death: endangering California and Oregon forest ecosystems. Frontiers Ecol. Environ. 1 (5), 197–204.

Reich, R.M., Lundquist, J.E., 2005. Use of spatial statistics in assessing forest diseases. pp. 127–143. In: Lundquist, J.E., Hamelin, R.C. (Eds.), Forest Pathology: From Genes to Landscapes. American Phytopathological Society Press, St. Paul, MN, 175 pp.

Rizzo, D., Garbelotto, M., Davidson, J.M., Slaughter, G.W., Koike, S.T., 2002. Phytophthora ramorum as the cause of extensive mortality of Quercus spp. and *Lithocarpus densiflorus* in California. Plant Dis. 86 (3), 205–213.

Ripley, B.D., 1977. Modelling spatial patterns. J. R. Stat. Soc. Ser. B 39, 172–212.

Schurr, F.M., Bossdorf, O., Milton, S.J., Schumacher, J., 2004. Spatial pattern formation in semi-arid shrubland: a priori predicted versus observed pattern characteristics. Plant Ecol. 173, 271–282.

Smith, T.E., 2004. A scale-sensitive test of attraction and repulsion between spatial point patterns. Geogr. Anal. 36 (4), 315–331.

Stoyan, D., Stoyan, H., 1994. Fractals, Random Shapes and Point Field. John Wiley & Sons Ltd., England.

Suzuki, R.O., Kudoh, H., Kachi, N., 2003. Spatial and temporal variations in mortality of the biennial plant, *Lysimachia rubida*: effects of intraspecific competition and environmental heterogeneity. J. Ecol. 91, 114–125.

Vacek, S., Leps, J., 1996. Spatial dynamics for forest decline: the role of neighboring trees. J. Vegetation Sci. 7, 789–798.

Waagepetersen, R.P., 2007. An estimation function approach to inference for inhomogeneous Neyman–Scott processes. Biometrics 63, 252–258.

Welden, C., Slauson, W., Ward, R., 1990. Spatial pattern and interference in Pinon-Juniper woodlands of northwest Colorado. Great Basin Nat. 50 (4), 313–319.

Wu, X.B., Thurow, T.L., Whisenant, S.G., 2000. Fragmentation and changes in hydrologic function of tiger bush landscapes, south-west niger. J. Ecol. 88, 790–800.

Wulder, M.A., Hall, R.J., Coops, N.C., Franklin, S.E., 2004. High spatial resolution remotely sensed data for ecosystem characterization. BioScience 54, 511–521.